0026-895X/02/6102-463–472$3.00
MOLECULAR PHARMACOLOGY
Vol. 61, No. 2
1341/961620
Mol Pharmacol 61:463–472, 2002
Printed in U.S.A.

Mapping the Agonist Binding Site of the Nicotinic Acetylcholine Receptor by Cysteine Scanning Mutagenesis: Antagonist Footprint and Secondary Structure Prediction

DEIRDRE SULLIVAN, DAVID C. CHIARA, and JONATHAN B. COHEN

Department of Neurobiology, Harvard Medical School, Boston, Massachusetts

Received August 10, 2001; accepted November 6, 2001

This paper is available online at http://molpharm.aspetjournals.org

ABSTRACT

To further define the surface of the *Torpedo californica* nicotinic acetylcholine receptor (nAChR) contributing to the agonist binding site structure, we used the substituted Cys accessibility method to identify novel residues and determined the "footprint" of residues protected from modification by the reversible competitive antagonist *d*-tubocurarine (dTC). nAChRs containing single Cys substitutions within regions of the α- or γ-subunit primary structure known to contribute to the agonist binding site were expressed in *Xenopus laevis* oocytes. Cys substitutions in binding site segments A (αTyr-93 and αAsn-94), C (αTyr-198), and D (γGlu-57) had been shown previously to be accessible for modification. We now introduced cysteines from αAsp-195 to αIle-201 and from γAla-106 to γAsp-113 and identified positions accessible for modification in segments C (αAsp-195, αThr-196, αPro-197, αAsp-200, and αIle-201) and E (γAsn-107 and γLeu-109). dTC protected against alkylation in segments D (γGlu-57) and E (γLeu-109) but not in segment A (αTyr-93 and αAsn-94). In segment C, dTC protection experiments revealed a pattern in which every other residue (α196, α198, and α200, but not α197 or α201) was protected from alkylation. This pattern of protection provides evidence that bound dTC is near amino acids in segments C, D, and E but not in segment A, and identifies a β-strand surface within segment C contributing to the binding site. These results are discussed in terms of a homology model, based on the molluscan acetylcholine binding protein crystal structure, of the *T. californica* nAChR agonist binding site.

The binding sites for agonists and competitive antagonists in the nicotinic acetylcholine receptor (nAChR) are within the extracellular domain at the α-γ and α-δ subunit interfaces. Affinity labeling and mutagenesis studies have provided extensive evidence for a model of the agonist site structure with contributing amino acids from three distinct regions of the α-subunits (referred to as binding site segments A, B, and C) and from at least three regions of the γ (or δ)-subunit (segments D, E, and F) (reviewed in Prince and Sine, 1998; Arias, 2000; Corringer et al., 2000). Most features of the model are present in the binding site identified within the recently solved structure of a molluscan, glial-derived soluble ACh binding protein (AChBP), a homopentameric structural and functional homolog of the N-terminal ligand binding domain of a nAChR α-subunit (Brejc et al., 2001; Smit et al., 2001).

The substituted Cys accessibility method (Karlin and Akabas, 1998) has provided an alternative approach for characterizing structural features of the nAChR and other ion channels. An observed irreversible change in the functional properties of the channel, after exposure to a water-soluble sulfhydryl reagent, suggests that the substituted Cys is exposed at the water accessible protein surface. This technique has been used to identify the state-dependent accessibility of amino acids contributing to the ion conduction pathway of the nAChR (Akabas et al., 1994; Akabas and Karlin, 1995; Zhang and Karlin, 1997, 1998). In studies of the structure of the agonist binding site, which contains a disulfide bond between αCys-192/193 in segment C, most Cys substitutions are well tolerated within α184–198 and are accessible for modification (McLaughlin et al., 1995; Spura et al., 1999; Spura et al., 2000). Using Cys mutagenesis of *Torpedo californica* nAChR, we previously tested the accessibility of positions identified by affinity labeling and mutagenesis in segments A (αTyr-93), B (αTrp-149), C (αTyr-190 and αTyr-198), and D (γTrp-55 and γGlu-57) as well as surrounding amino acids in segments A (α90–96) and D (γ52–58) and found that αTyr-93, αAsn-94, αTyr-198, and γGlu-57 were accessible (Sullivan and Cohen, 2000). That study also

This research was supported in part by United States Public Health Service grant NS19522 (J.B.C.) and by a Muscular Dystrophy Association Research Development grant (D.S.).

ABBREVIATIONS: nAChR, nicotinic acetylcholine receptor; ACh, acetylcholine; AChBP, acetylcholine binding protein of *Lymnaea stagnalis*; MTSET, ([2-(trimethylammonium)-ethyl]-methanethiosulfonate; dTC, d-tubocurarine; MTSEA, 2-aminoethylmethanethiosulfonate; MTSPT, [3-(trimethylammonium)propyl]-methanethiosulfonate; MBTA, 4-(N-maleimido)benzyltrimethylammonium.

helped to define the structural requirements for ligand orientation compatible with nAChR activation, as [2-(trimethylammonium)-ethyl]-methanethiosulfonate (MTSET), which attaches thiocholine, acted as an irreversible antagonist at positions αY93C and γE57C but as a covalent agonist at αY198C. Furthermore, a structural analog with the tethering arm shortened by one methylene group (0.7 Å) acted as an irreversible antagonist at αY198C and at all other accessible positions.

In this report, we extended these studies by identifying additional accessible residues in segment C (α195–201) as well as segment E (γ106–113), which includes residues identified by photoaffinity labeling with the antagonists [^{3}H]4-benzoylbenzoylcholine (γLeu-109; Wang et al., 2000) and [^{3}H]*d*-tubocurarine (dTC) (γTyr-111; Chiara et al., 1999). With these mutant nAChRs, we also tested whether MTSET or its analogs could act as irreversible agonists when tethered at positions other than αY198C. In addition, we used the panel of nAChR binding site mutants containing accessible cysteines to identify positions that could be protected from alkylation when the agonist binding site was occupied by dTC. Based upon photoaffinity labeling, [^{3}H]dTC binds to the agonist site at the α-γ interface near amino acids in segments C (αTyr-190, αCys-192, and αTyr-198), D (γTrp-55), and E (γTyr-111 and γTyr-117; Chiara and Cohen, 1997; Chiara et al., 1999), and dTC can protect against MTSET reaction at αY198C (Sullivan and Cohen, 2000). The results we now report, which indicate protection of alkylation of positions in segments C, D, and E but not in segment A, are consistent with the results of photoaffinity labeling. The pattern of protected residues within segment C indicates that this region is organized as a β-strand and identifies a surface projecting toward the ACh binding site consistent with the structure of the binding site in the AChBP (Brejc et al., 2001). However, the lack of protection of αY93C is surprising in terms of that structure. Our experimental results are compared with a homology model of the *T. californica* agonist binding site based on the crystal structure of the AChBP and are generally consistent with this structure. However, the accessibility of some residues suggests differences between the model and the structure of the *T. californica* nAChR binding site in the absence of agonist (our experimental conditions).

Materials and Methods

cDNA Mutagenesis. Mutants were constructed by "overlap extension" PCR using *T. californica* nAChR subunit plasmids (α, γ, and δ in pMXT and β in pSP64) and reagents as described previously (Sullivan and Cohen, 2000). The mutations of amino acids 195–201 of the mature α-subunit were generated using primers which gave a PCR product of ~1000 base pairs that could be subcloned using the unique *Bsi*WI restriction site and the *Bbv*II site near the 3′ end of the α-subunit coding region. Mutations of amino acids 106 to 113 in the mature γ-subunit were made by generating a PCR product of ~1.13 kilobases that was subcloned using the unique *Hin*dIII site in the vector and the *Stu*I site in the γ-subunit coding region. Each PCR mix contained 0.5 μM primers, 50 ng of template DNA, and 0.4 mM dNTPs in the reaction buffer supplied with the enzyme. PCR reactions were for 24 cycles with a three-step protocol (1.5 min at 95°C, 45°C, and 72°C).

Electrophysiology. *T. californica* nAChR subunit-specific cRNAs were transcribed in vitro and *Xenopus laevis* oocytes were injected as described previously (Sullivan and Cohen, 2000). Isolated, follicle-free oocytes were injected with 0.5 to 10 ng of subunit-specific RNAs in a molar ratio of 2α/β/γ/δ, and currents elicited by ACh were measured 48 to 72 h after injection by two-electrode voltage clamp. Under our experimental conditions, for oocytes injected with 0.5 ng of wild-type nAChR subunit cRNAs, maximal current responses for ACh were typically 1 to 2 μA. For the Cys substitutions between α195 and α201 in segment C, the maximal current responses for ACh were similar to wild-type for the mutant nAChRs containing Cys at α195, α196, α197, or α199. As described previously, the αY198C nAChRs showed maximal current levels ~1% of wild-type, and for the αD200C and αI201C mutant nAChRs, the maximal currents were also 1 to 5% of wild-type. For αY198C, as judged by binding of ^{125}I-α-bungarotoxin to intact oocytes, surface nAChR levels were ~50% of wild-type. Within segment E (γ106–113), the maximal ACh current responses were similar to wild-type for each substitution except for γY111C, which had maximal responses ~2% of wild-type and surface nAChR levels <10% of wild-type. Surface receptor expression levels of other mutants were not quantified. Salts, atropine, ACh, and dTC were from Sigma (St. Louis, MO). MTSET, [3-(trimethylammonium)-propyl]-methanethiosulfonate (MTSPT), 2-aminoethylmethanethiosulfonate (MTSEA), and 4-(*N*-maleimido)benzyltrimethylammonium (MBTA) were from Toronto Research Chemicals (North York, Ontario, Canada), and Biotin-PEO-maleimide (Fig. 1) was from Pierce (Rockford, IL). Sulfhydryl-modifying reagents were prepared as millimolar stock solutions in recording solution and stored on ice during use, with fresh solutions prepared approximately every 2 h. For nAChR activation, ACh dose response curves were fit to the equation: $I / I_{max} = [1 + (K_{app} / [ACh])^{n_H}]^{-1}$, where I and I_{max} are the currents at a given concentration of ACh and the maximal current, respectively. K_{app} is the apparent activation constant for ACh and n_H is the Hill coefficient. pCLAMP (Axon Instruments, Foster City, CA) and SigmaPlot (SPSS Inc., Chicago, IL) software were used for data analysis.

Rate Constants of nAChR Modification. For the sulfhydryl-reactive reagents producing irreversible inhibition of ACh responses, the time course of the reaction with a substituted Cys mutant in the absence of ACh was determined by recording the initial response to ACh and then the response to ACh after repeated applications of

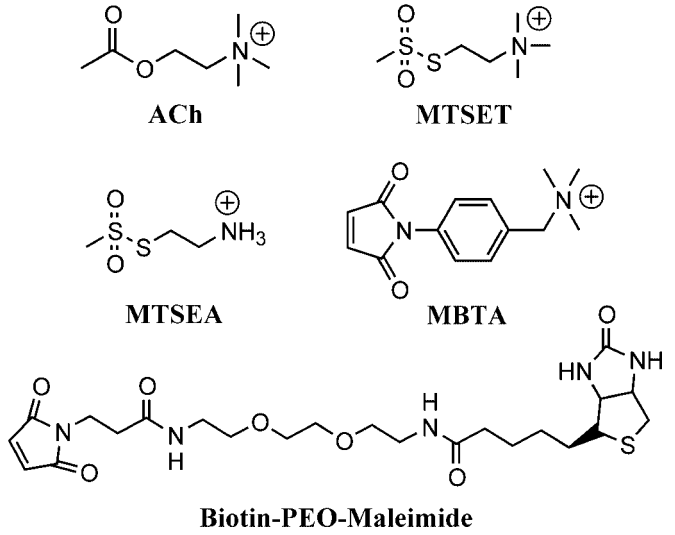

Fig. 1. Structures of sulfhydryl-modifying reagents. The extended length of ACh measures 8.7 Å. Reaction with MTSEA transfers to the Cys sulfur the primary amine 2-aminoethanethiol, which, in an extended conformation, extends 5.8 Å from the point of attachment to the surface of the primary amine group. Reaction with MTSET transfers thiocholine, which can extend 6.9 Å from the Cys sulfur to the surface of the trimethylammonio group. MBTA positions the trimethylammonio group 12.2 Å from the point of attachment. Biotin-PEO-maleimide has an extended length of 29 Å.

modifying reagent for 5-s intervals. Each application of reagent was followed by a ~1-min wash, three ACh test applications (5 s each), and a 1-min wash. ACh was generally applied at a concentration equal to K_{app}. ACh-induced currents after treatment were plotted as a function of cumulative modification time (t) and fit by a single exponential function, $I_t = I_\infty + (I_o - I_\infty) \exp(-t / \tau)$ where I_t is the current at a given time, I_∞ is the amount of current remaining after the reaction is complete, and I_o is the initial current level. $1 / \tau$ is the pseudo–first-order rate constant and the second-order rate constant, k, is $(1 / \tau) / x$, where x is the concentration of modifying reagent.

dTC Protection Assay. Responses to ACh at a concentration near K_{app} were measured before and after coapplication of dTC and ACh to show that 10 μM dTC was sufficient to reversibly block >95% of the ACh response and that the Cys substitution itself had not interfered with the receptors' ability to bind dTC. This initial part of the assay was also necessary to determine that the effects of dTC were reversible. It was often necessary to wash the oocyte for several minutes after dTC application for full recovery of the ACh response. To measure the degree of protection by dTC, ACh test pulses were measured before and after 10 μM dTC was coapplied with a concentration of MTSET known to cause 50 to 80% inhibition (based on rate constants). The same concentration of MTSET was then applied in the absence of dTC, again using ACh test pulses to measure the extent of inhibition. The degree of protection was then determined by comparing the ratio of the extent of modification in the absence of dTC to the extent of modification in the presence of dTC: % protection = $[1 - (\%\ \text{Inhibition}_{dTC/MTSET} / \%\ \text{Inhibition}_{MTSET})] \times 100$.

Homology Modeling of the *T. californica* nAChR. Molecular modeling of the extracellular domain of the *T. californica* nAChR based upon the recently published structure of the AChBP (Brejc et al., 2001) was done using Insight II (Version 98; MSI, San Diego, CA) on a Silicon Graphics O_2 workstation. The sequences for the four *T. californica* nAChR subunits (NCB accession numbers: ACRYA1, ACRYB1, ACRYG1, and ACRYD1) were obtained from the National Center for Biotechnology Information and the coordinates for the structure of the AChBP (PDB number 1I9B) were obtained from the Research Collaboratory for Structural Bioinformatics (http://www.rcsb.org). The nAChR subunit sequence alignment presented by Brejc et al. (2001) was used, and the AChBP structure was examined to ensure that insertions and deletions occurred within exposed flexible segments. The Insight II Homology module placed the nAChR sequences into the AChBP structure and the Insight II Discovery module energy minimized the resulting structural model. Compared with the primary structure of the AChBP, the nAChR α-subunit contains insertions in two regions within the ACh binding site. Although segment C in all neuronal nAChR α-subunits aligns well with the AChBP, the *T. californica* and skeletal muscle α-subunits contain a single residue insertion between αCys-193 and αTyr-198. We designated αAsp-195 as the inserted residue to preserve the β10-strand beginning at αThr-196, with αThr-196, αTyr-198, and αAsp-200 projecting in the direction of the binding site, a structure consistent with experimental results described in this report. The other α-subunit insertion in the vicinity of the binding site was αAla-96 in segment A. Both insertions were well tolerated upon minimization.

The only region of nAChR subunit primary structure which was not a straightforward substitution or small segment insertion was the poorly aligned region encompassing the amino acids of binding site segment F. This region of primary structure required insertions of 9, 7, and 11 amino acids in the β-, γ-, and δ-subunits, respectively, in the segment region between the β8 and β9 β-strands. Lacking additional guidelines, we placed these insertions (β164–172, γ164–170, and δ166–176) in external loops to preserve the structure of the adjacent regions that were homologous to the AChBP sequence. In our model, γSer-161, which has been identified as a dTC selectivity determinant for mouse nAChR (Sine, 1993), occurs just after the β8-strand and is positioned beyond γLys-34, ~15 Å from the center of the aromatic binding pocket. Similarly, γGlu-183, which was identified as a determinant of agonist K_{app} (Czajkowski et al., 1993), occurs at the NH_2 terminus of the β9-strand, which would lie near the plane of the membrane in a nAChR, 26 Å from the agonist binding site. γAsp-177 is positioned outside of αTyr-190/γTrp-55, closer to the binding pocket than γAsp-174, an important determinant of agonist K_{app} (Martin et al., 1996; Martin and Karlin, 1997). Because segment F residues seem more distantly related to the core structure of the binding site and amino acids in this region have not been examined in this study, the predicted positions of these residues are not included in our model of the *T. californica* nAChR ACh binding site.

In the AChBP structure, a HEPES molecule was identified within the aromatic pocket of the ACh binding site. We placed ACh molecules into the equivalent positions of our nAChR model (at the α-γ and α-δ interfaces) using the Insight II Docking module, and the structure containing the ACh molecules was energy minimized. A single orientation for each ACh molecule was favored (docking energy of −30 kcal), which placed the ACh nitrogen within the aromatic pocket of the ligand binding site consisting of αTyr-93, αTrp-149, αTyr-190, αTyr-198, and γTrp-55/δTrp-57.

Results

Functional Properties of nAChRs with Cys Substitutions in Binding Site Segments C and E. nAChR functional properties were assessed by measuring ACh-elicited currents using two-electrode voltage clamp. Each of the substitutions within α195–α201 and γ106–γ113, when expressed with other wild-type subunits, resulted in functional nAChRs (Table 1). For wild-type nAChR, the K_{app} for ACh was 30 ± 8 μM. For the segment C mutant nAChRs, there was a significant rightward shift of K_{app} only for the Cys substitution at αY198C. The mutant nAChRs with substituted Cys adjacent to αTyr-198 at either αPro-197 or αLeu-199 were characterized by leftward shifts of K_{app}, whereas for the other substitutions studied in this segment, the K_{app} values were shifted <2-fold compared with wild-type. The Cys substitutions in segment E (γ106–γ113) were also well tolerated. The largest shifts of K_{app} were seen for the γL109C (K_{app} = 100 μM) and γY111C (K_{app} = 14 μM) mutants, whereas for substitutions at each of the other positions, K_{app} for ACh was within a factor of 2 of wild-type.

Modification of Substituted Cysteines within Binding Site Segment C. For oocytes expressing wild-type or mutant nAChRs, the response to ACh was measured at a concentration close to K_{app}. Oocytes were then exposed to MTSET (200 μM), MTSEA (1 mM), or maleimide-PEO-biotin

TABLE 1

Functional properties of binding site segment C and E mutant nAChRs

Macroscopic dose response curves were measured as described under *Materials and Methods* with the tabulated K_{app} representing the mean ± S.D. determined from at least three oocytes. For wild-type nAChR, n_H = 1.6 ± 0.1, and the Hill coefficients for the Cys mutants, measured in the same manner, were not significantly different from wild-type.

Segment C		Segment E	
nAChR	K_{app}	nAChR	K_{app}
	μM		μM
Wild type	30 ± 8	γA106C	23 ± 2
αD195C	35 ± 13	γN107C	34 ± 14
αT196C	21 ± 9	γV108C	32 ± 8
αP197C	5.1 ± 0.6	γL109C	102 ± 18
αY198C	860 ± 50	γV110C	28 ± 7
αL199C	4.0 ± 1.6	γY111C	14 ± 7
αD200C	34 ± 3	γN112C	47 ± 28
αI201C	20 ± 8	γD113C	56 ± 25

(1 mM) (Fig. 1) for 5 s in the absence of agonist; after a wash of 1 to 2 min, the ACh response was remeasured. Representative current traces are shown for wild-type and segment C mutant nAChRs treated with MTSET (Fig. 2A), and summary data for each of the mutants are presented for the effects of MTSET, MTSEA, and maleimide-PEO-biotin (Fig. 2B). We were particularly interested in determining whether thiocholine tethered at positions other than αY198C in segment C would result in covalent activation. However, treatment with MTSET for 5 s resulted in irreversible inhibition of the ACh response by >75% for the αT196C, αP197C, and αD200C mutant nAChRs, and a smaller inhibition of the αI201C mutant that increased with longer reaction times (see later). The ~10% inhibition of the αD195C or αL199C mutants was less than that seen for wild-type nAChR and was not indicative of modification of the substituted Cys. Treatment with MTSEA also resulted in irreversible inhibition of ACh current responses for those mutants sensitive to MTSET. Modification with maleimide-PEO-biotin (1 mM, 5 s) significantly inhibited the ACh responses for the same mutants and, in addition, it inhibited irreversibly the αD195C nAChR mutant.

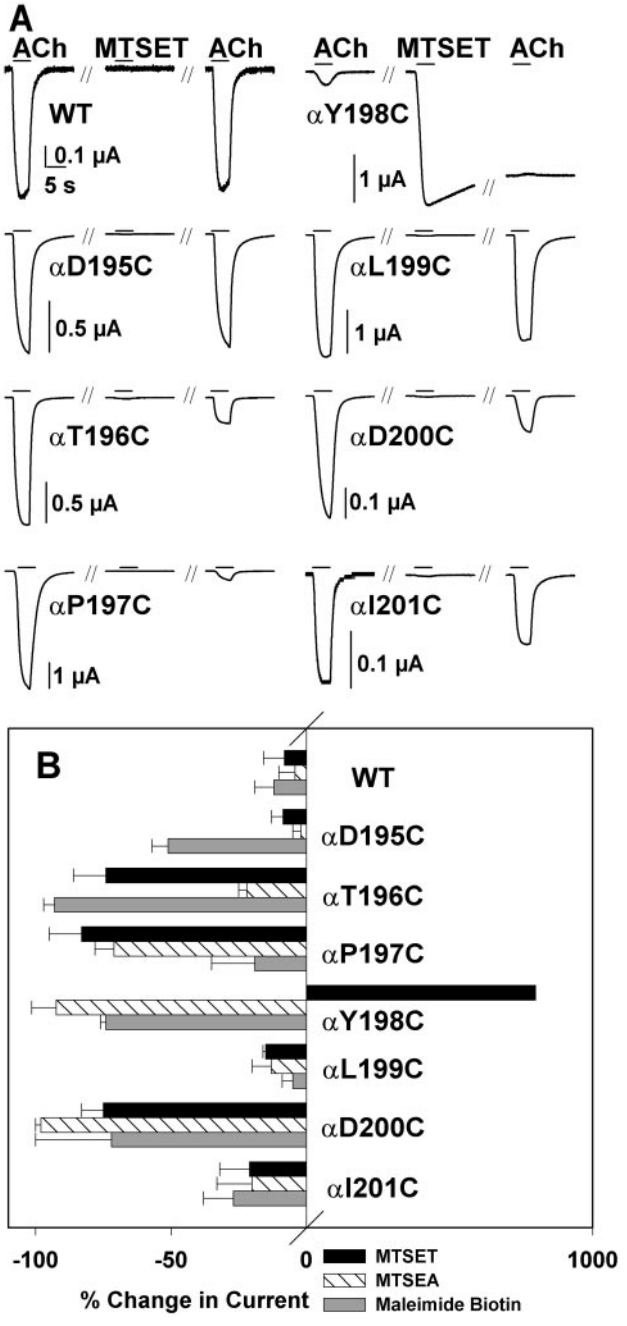

Fig. 2. Effects of MTSET, MTSEA, and Maleimide-PEO-Biotin on nAChRs containing Cys substitutions in binding site segment C. A, current responses (microamperes) of nAChRs to ACh were determined before and after a 5-s application of 200 μM MTSET. ACh test concentrations were near K_{app}: (WT, 10 μM; αD195C, 30 μM; αT196C, 30 μM; αP197C, 3 μM; αY198C, 1000 μM; αL199C, 3 μM; αD200C, 30 μM; αI201C, 30 μM). Horizontal scale bar is 5 s. B, the mean change in current was determined by testing oocytes with at least three applications of a half-maximal concentration of ACh before and after a 5-s application of 200 μM MTSET (■), 1 mM MTSEA (▨), or 2 mM maleimide-PEO-biotin (▤). Bars represent the mean change in current ± S.D. from experiments on at least three oocytes. Percentage change in current was calculated as: $[(I_{after\ MX} / I_{before} - 1)] \times 100$.

To look further for the possibility of channel activation, we also tested the effects of MTSPT, which is one methylene group longer than MTSET, reasoning that the quaternary ammonium attached to a longer tethering arm might act as an agonist if attached at other positions in proximity to αTyr-198 (data not shown). MTSPT confirmed the accessibility of residues αT196C, αP197C, and αD200C by inhibiting subsequent ACh responses, but it only activated the αY198C mutant, as described previously (Sullivan and Cohen, 2000).

Modification of Substituted Cysteines within Binding Site Segment E. Cys substitutions at γ106 to γ113 were similarly tested for their sensitivity to MTSET and MTSEA (Fig. 3). Summary data show that a 5-sec exposure to MTSET (200 μM) or MTSEA (1 mM) inhibited ACh responses for the γN107C mutant by ~30 and 75%, respectively, whereas both compounds inhibited the γL109C response by ~90%. Effects at the other positions tested were not sufficiently different from wild-type to make any conclusions about their accessibility. Exposure of these mutants to maleimide-PEO-biotin

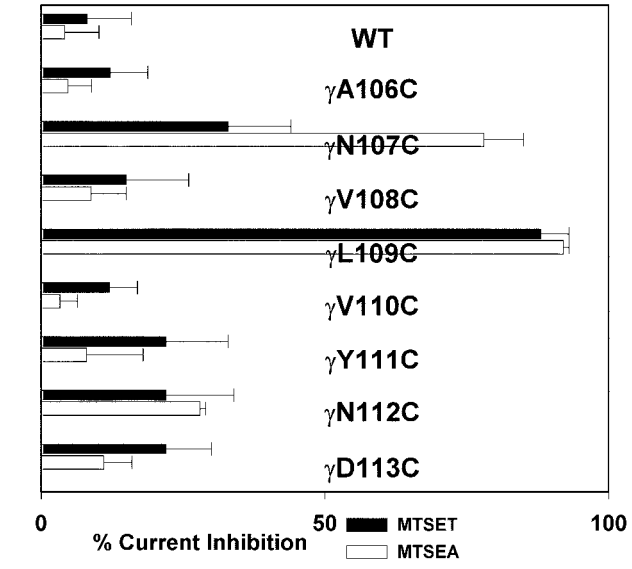

Fig. 3. Effects of MTSET and MTSEA on nAChRs containing Cys substitutions in binding site segment E. MTSET (■) and MTSEA (□) current inhibition was determined as in Fig. 2B. ACh test concentrations, which were near K_{app}, were 30 μM except for γαL109C, which was tested at 100 μM. Percentage current inhibition was defined as: $[1 - (I_{after\ MX} / I_{before})] \times 100$. Each bar represents the mean ± S.D. from experiments on at least three oocytes.

did not yield any additional information about residue accessibility (data not shown).

Reaction Rate Constants. The rates of reaction were measured to determine the effect of full modification at a particular residue in response to a specific reagent and to give us the kinetic information necessary to design protocols for subsequent dTC protection experiments. For the Cys mutants inhibited irreversibly by MTSET or MTSEA, the rates of reaction with mutant nAChRs were determined by measuring the response to ACh after increasing reaction times and for various reagent concentrations (Fig. 4). For oocytes expressing αY93C, αY198C, and γE57C nAChRs, ACh responses were inhibited by >90% after full modification (Sullivan and Cohen, 2000). In contrast, even after complete modification, the ACh current response was not fully inhibited for a number of the segment C and E Cys mutants characterized here. For αT196C and αI201C mutant nAChRs, ACh current responses were maximally inhibited 30 to 50% by MTSEA, whereas αP197C and αD200C responses were inhibited by 75% and 95%, respectively (Fig. 4A). For substitutions in segment E, MTSEA treatment inhibited γN107C responses by 80%, whereas it inhibited γL109C responses by >90% (Fig. 4B), similar to the level of inhibition seen for the γE57C mutant. MTSET treatment of αT196C nAChRs resulted in maximal inhibition of 80% (Fig. 4C), compared with the maximal inhibition of 30% seen after reaction with MTSEA. MTSET also more fully inhibited responses at αP197C than MTSEA. MTSET treatment inhibited to the same extent as MTSEA at αD200C (>90%) and αI201C (50%). For substitutions in the γ-subunit, MTSET fully inhibited the γE57C and γL109C nAChR, whereas for the γN107C nAChR, maximal inhibition was only 50% (Fig. 4D).

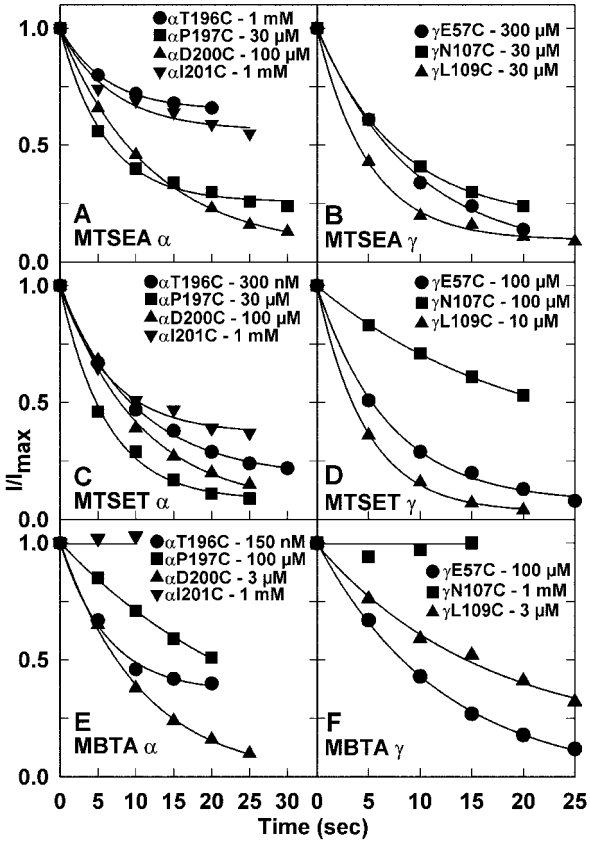

Fig. 4. Kinetics of modification of nAChRs with Cys substitutions in binding site segments C, D, or E by MTSEA, MTSET, and MBTA. Symbols represent the fraction of residual current response plotted as a function of cumulative modification time. ACh responses were measured before and after each 5-s application of reagent and were normalized to the initial response. Plots were fit with single exponential functions as described under *Materials and Methods* to give the first-order rate constant $1/\tau$ (s^{-1}) and the fractional response remaining after full modification, I_∞. A, MTSEA modification rates are shown for segment C residues: αT196C, 1 mM (τ = 6 s, I_∞ = 0.65); αP197C, 30 μM (τ = 6 s, I_∞ = 0.26); αD200C, 100 μM (τ = 13 s, I_∞ = 0.06); αI201C, 1 mM (τ = 8 s, I_∞ = 0.56). B, MTSEA modification rates are shown for γ-subunit Cys substitutions in binding site segments D and E: γE57C, 300 μM (τ = 10 s, I_∞ = 0); γN107C, 30 μM (τ = 8 s, I_∞ = 0.13); γL109C, 30 μM (τ = 5 s, I_∞ = 0.09). C, MTSET modification rates are shown for segment C residues: αT196C, 300 nM (τ = 10 s, I_∞ = 0.18); αP197C, 30 μM (τ = 6 s, I_∞ = 0.08); αD200C, 100 μM (τ = 12 s, I_∞ = 0.06); αI201C, 1 mM (τ = 7 s, I_∞ = 0.37). D, MTSET modification rates for γ-subunit: γE57C, 100 μM (τ = 8 s, I_∞ = 0.07); γN107C, 100 μM (τ = 22 s, I_∞ = 0.18); γL109C, 10 μM (τ = 5 s, I_∞ = 0.09). E, MBTA modification rates are shown for segment C residues: αT196C, 150 nM (τ = 6 s, I_∞ = 0.36); αP197C, 100 μM (τ = 26 s, I_∞ = 0.03); αD200C, 3 μM (τ = 11 s, I_∞ = 0); αI201C, 1 mM (not fit). F, MBTA modification rates for γ-subunit segment D and E residues: γE57C, 100 μM (τ = 12 s, I_∞ = 0); γN107C, 1 mM (not fit); γL109C, 3 μM (τ = 17 s, I_∞ = 0.15). Parameter uncertainties were 5 to 20% for τ and 1 to 15% for $I\infty$.

We also examined the kinetics of modification of the mutant nAChRs by MBTA (Fig. 1), the alkylating antagonist used (Kao et al., 1984) to identify αCys-192/193 as amino acids of the agonist binding site in the *T. californica* nAChR (after disulfide reduction). Reaction with MBTA at αT196C, αP197C, αD200C, and γL109C resulted in irreversible inhibition of the ACh responses to the same extent as seen after modification with MTSET (Fig. 4, E and F). αI201C and γN107C (Fig. 4, E and F) nAChRs, although sensitive to MTSEA and MTSET, were not inhibited after exposure to MBTA, suggesting that MBTA modification may be more orientation-dependent.

The apparent bimolecular reaction rate constants for MTSEA, MTSET, or MBTA modification of the mutant nAChRs (Table 2) were determined from the rates of reaction, which increased with increasing reagent concentration. While the reaction rate constants at αY93C, αY198C, and

TABLE 2

Modification reaction rate constants of mutant nAChRs by MTSEA, MTSET, and MBTA

Reaction rate constants, k (mM^{-1} sec^{-1}), were determined as described under *Materials and Methods* and in Fig. 4 from experiments on 2 to 8 oocytes.

nAChR	*k*			dTC Protection
	MTSEA	MBTA	MTSET	
Segment A				
αY93C[a]	2.9 ± 0.7	0.6 ± 0.1	6.4 ± 3.1	–
αN94C	0.17 ± 0.04	0.07 ± 0.02	5.4 ± 1.6	–
Segment C				
αD195C	N.D.	N.D.	N.D.	N.D.
αT196C	0.20 ± 0.04	1010 ± 260	240 ± 90	+
αP197C	4.3 ± 1.4	0.3 ± 0.1	7.1 ± 2.1	–
αY198C[a]	230 ± 40	5.4 ± 1.4	210 ± 10	+
αL199C	N.D.	N.D.	N.D.	N.D.
αD200C	1.1 ± 0.6	56 ± 31	0.9 ± 0.1	+
αI201C	0.14 ± 0.01	N.D.	0.18 ± 0.05	–
Segment D				
γE57C[a]	0.4 ± 0.1	0.8 ± 0.2	1.0 ± 0.5	+
Segment E				
γN107C	3.7 ± 0.9	N.D.	0.4 ± 0.2	N.D.
γL109C	8.9 ± 2.0	23 ± 14	17 ± 8	+

[a] Rate constants from (Sullivan and Cohen, 2000).
N.D., not determined due to lack of effect of reagent on ACh response.

γE57C differed by as much as 500-fold, at each position, the rate constants for MTSEA and MTSET differed by <2-fold, and the rate constants for MBTA were never larger than for MTSET. For the other positions tested within segment C, the rate constants for MTSET (or MTSEA) varied by ~100-fold without any characteristic periodicity, and the rate constants for MBTA varied by as much as 3000-fold at adjacent amino acids (αT196C, αP197C). At αT196C, MTSET ($k \sim 2 \times 10^5$ M^{-1} s^{-1}) reacted ~1000-fold faster than MTSEA, whereas at the other positions examined, the rate constants for the two compounds differed by <2-fold. Whereas the rate constant for MBTA reaction with αY198C ($k \sim 5 \times 10^3$ M^{-1} s^{-1}) was only 2% of that for MTSET, for αT196C the rate constant for MBTA ($k \sim 1 \times 10^6$ M^{-1} s^{-1}) was 5-fold higher than that for MTSET and similar to the rate constant for MBTA modification of αCys-192/193 in reduced, native *T. californica* nAChR ($k \sim 3 \times 10^6$ M^{-1} s^{-1}) (Stauffer and Karlin, 1994). At αD200C the rate constant for MBTA ($k \sim 5 \times 10^4$ M^{-1} s^{-1}) was 50-fold higher than for MTSET. Within segment E, the rate constant for MTSET reaction at γL109C ($k \sim 2 \times 10^4$ M^{-1} s^{-1}) was 40-fold greater than at γN107C, and for γL109C or γE57C nAChRs the rate constants for MTSEA, MTSET and MBTA were essentially the same.

Effects of Alkylation on ACh Dose Response. Analysis of the kinetics of MTSET modification of the mutant nAChRs revealed that after full modification, ACh responses were inhibited by ≥90% at some positions (αY93C, αP197C, αD200C, γE57C, γL109C) but not at others (αT196C, αI201C). For the latter positions, it was clear that the tethered thiocholine modified the ACh response but did not prevent ACh binding. Additional experiments were carried out to determine whether, at the other positions, tethered thiocholine acted as an irreversible antagonist or alternately as a modifier of ACh binding and/or gating. We characterized ACh dose response curves before and after modification to determine whether the inhibition seen at a fixed concentration of ACh resulted from reduction only of the maximal response or also from a modification of K_{app}. If modification resulted in a nAChR no longer capable of being activated by ACh, then any ACh induced currents could result only from remaining unmodified nAChRs, and the response after exposure to MTSET would be characterized by a decreased maximal current without change of K_{app}. For example, modification of αY93C or γE57C nAChRs by MTSET or MTSEA resulted in reductions of maximum current without change of K_{app} (Sullivan and Cohen, 2000). If after modification, ACh was still able to gate the ion channel, but with either the binding or gating altered, then the response could be characterized by a shift of K_{app}.

For the two positions apparently insensitive to MTSET (αD195C and αL199C), the shifts of the ACh dose response curves after MTSET treatment (~20% reduction of maximal response, K_{app} shift <1.5-fold) were similar to the effects of MTSET on wild-type nAChR (Fig. 5, A and B; data not shown). For two positions with substantial responses after full modification (αT196C and αI201C), K_{app} values were shifted by <2-fold (Fig. 5, A and C). The αP197C nAChR was inhibited by >90% when tested at 30 μM ACh (Fig. 4C). This inhibition resulted from a 10-fold increase in K_{app} with less than a 20% reduction of the maximal response (Fig. 5B). After full modification of the αD200C mutant, the maximal response was reduced by only 80% and the K_{app} value increased 2-fold (Fig. 5C). Thiocholine tethered at αT196C, αP197C, αD200C, or αI201C altered either ACh binding or gating, but did not act as a covalent antagonist that prevented the binding of ACh.

For substitutions in the γ-subunit, modification of either γE57C or γL109C can cause >90% inhibition of the ACh response when tested at a concentration near K_{app} (Fig. 4D). For the γE57C mutant, limited modification of nAChRs by exposure to 100 μM MTSET for 5 s resulted in a 70% reduction of maximal response with no shift of K_{app} (Fig. 5D). Treatment of the γL109C mutant with 200 μM MTSET for 5 s, which was sufficient for maximal modification (Fig. 4D), resulted in a reduction of the maximum response by only 70% accompanied by a 3- to 4-fold increase in K_{app} (Fig. 5D). Thus, with thiocholine tethered at γL109C, ACh was still able to bind and gate the ion channel.

dTC Protection Experiments. From our previous work and the experiments presented here, we identified accessible residues in ACh binding site segments A (αY93C and αN94C), C (αD195C, αT196C, αP197C, αY198C, αD200C, and αI201C), D (γE57C), and E (γN107C and γL109C). However, the fact that modification of the substituted cysteines led to altered ACh responses does not establish that these positions actually contribute to the structure of the ACh binding site. The altered responses could result from an allosteric modification of the structure of the binding site or

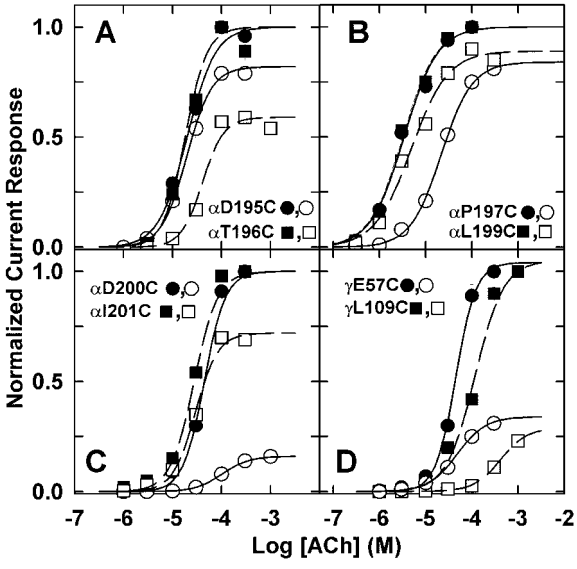

Fig. 5. ACh dose response curves before (filled symbols) and after (open symbols) reaction with MTSET. A, data were fit as described under *Materials and Methods*. Responses were normalized to the maximal response for each oocyte. A, αD195C (solid lines): K_{app} = 20 μM, n_H = 1.5; after 200 μM MTSET, 5 s: K_{app} = 20 μM, I_{max} = 0.82. αT196C (dotted lines): K_{app} = 18 μM, n_H = 2.0, after 1 mM MTSET, 15 s: K_{app} = 41 μM, I_{max} = 0.59. B, αP197C (solid lines): K_{app} = 3.4 μM, n_H = 1.2; after 1 mM MTSET, 10 s: K_{app} = 22 μM, I_{max} = 0.84. αL199C (dotted lines): K_{app} = 3.2 μM, n_H = 1.2; after 1 mM MTSET, 10 s: K_{app} = 4.9 μM, I_{max} = 0.89. C, αD200C (solid lines): K_{app} = 44 μM, n_H = 2.0; after 1 mM MTSET, 10 s: K_{app} = 103 μM, I_{max} = 0.16. αI201C (dotted lines): K_{app} = 28 μM, n_H = 1.9; after 1 mM MTSET, 10 s: K_{app} = 29 μM, I_{max} = 0.72. D, γE57C (solid lines): K_{app} = 44 μM, n_H = 2.0; after 100 μM MTSET, 5 s: K_{app} = 47 μM, I_{max} = 0.34. γL109C (dotted lines): K_{app} = 116 μM, n_H = 1.4; after 200 μM MTSET, 5 s: K_{app} = 400 μM, I_{max} = 0.29. Each point represents the mean ± S.D. for at least three measurements. Parameter uncertainties were 5 to 20% of K_{app} or n_H and <10% for I_{max}. Values of n_H were unchanged after modification, with the exception of γE57C, for which n_H decreased from 2.0 to 1.4.

from a perturbation of the conformational transition necessary for channel gating. If MTSET is within the agonist binding site when it reacts with a substituted Cys, then that reaction should be inhibited by the presence of a reversible agonist or antagonist that is bound in proximity to that position.

We used the competitive antagonist dTC to initially characterize the effects of cholinergic drugs on the modification by MTSET. When applied with an ACh concentration causing ~50% maximal response, we found that 10 μM dTC was sufficient to block >95% of the ACh responses for the wild-type and the Cys mutant nAChRs, with >90% recovery from inhibition when the ACh response was retested after a wash of 1 to 2 min (data not shown). To measure the degree of protection by dTC, ACh test pulses were determined before and after 10 μM dTC was coapplied for 5 s with a concentration of MTSET known to cause 50 to 80% inhibition. The same concentration of MTSET was then applied for 5 s in the absence of dTC, again using ACh test pulses to measure the extent of inhibition.

Representative current traces for dTC protection experiments are shown for residues in segments A, D, and E (Fig. 6, left) and for segment C (Fig. 6, right). ACh responses for wild-type nAChRs did not change after dTC/MTSET or MTSET application. dTC at 10 μM did not prevent reaction of MTSET at residue αY93C. αY93C nAChRs were inhibited by ~90% when MTSET was applied in the presence of dTC, and the remaining ACh response was inhibited by a further treatment by MTSET alone. Similarly, dTC did not prevent reaction of MTSET with αN94C (not shown). In contrast, for γE57C in segment D, γL109C in segment E, and for some of the positions in segment C, dTC did protect against modification by MTSET. dTC provided 90% protection of the γE57C and γL109C nAChRs. For example, for γE57C, the ACh response was inhibited by only 7% after the oocyte was perfused with MTSET in the presence of dTC and then inhibited by 75% after perfusion with MTSET alone.

Similar protection experiments were done for the segment C residues accessible to MTSET modification (Fig. 6, right).

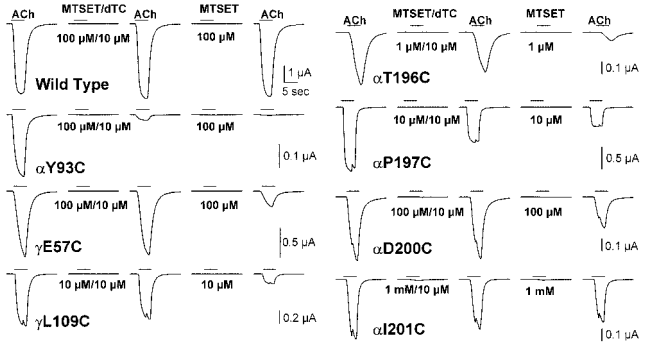

Fig. 6. Competitive antagonist protection of MTSET alkylation of reactive Cys residues. To measure the degree of protection by 10 μM dTC, current responses to ACh at a concentration near K_{app} were measured before and after 10 μM dTC was coapplied for 5 s with a concentration of MTSET known to cause 50 to 80% inhibition. The same concentration of MTSET was then applied for 5 s in the absence of dTC, again using ACh test pulses to measure the extent of inhibition. The degree of protection was defined as $[1 - (\%\ \text{Inhibition}_{\text{dTC/MTSET}} / \%\ \text{Inhibition}_{\text{MTSET}})] \times 100$. Current traces are shown from oocytes expressing wild-type and nAChRs with substitutions in segments A (αY93C), D (γE57C), and E (γL109C) (left) and segment C (αT196C, αP197C, αD200C, and αI201C) (right). Horizontal scale bar is 5 s.

Because of the high reaction rate constant for MTSET modification of αT196C, MTSET was used at 1 μM for that position. Consistent with lower rate constants for modification of the other positions (Table 2), MTSET was tested at 10 μM for αP197C, at 100 μM for αD200C, and at 1 mM for αI201C. dTC protected against MTSET modification at αT196C and αD200C but not at αP197C and αI201C. For the αT196C receptor, dTC protected by ~80% in the experiment shown in Fig. 6; in two additional experiments, dTC protected αT196C by ~60%. For the αD200C receptor in the experiment shown (Fig. 6) and in an additional experiment, dTC protected by 80 to 90%. dTC did not protect the αP197C nAChR from modification: there was ~40% inhibition of the ACh response after treatment with MTSET in the presence or absence of dTC. Similarily, dTC did not protect the αI201C nAChR from modification. Exposure to 1 mM MTSET for 5 s in the presence of dTC caused ~20% inhibition of the subsequent αI201C ACh response, whereas application of 1 mM MTSET alone caused only a further 10% inhibition of the ACh response. Because there was more inhibition after exposure to MTSET in the presence of dTC than in its absence, we conclude that dTC afforded no protection at αI201C. Thus, within segment C, dTC binding protected against alkylation at αT196C, αY198C (previously shown), and αD200C, but not at αP197C or αI201C.

A Homology Model of the *T. californica* nAChR Binding Site. The studies described above were carried out before the publication of the structure of the molluscan AChBP (Brejc et al., 2001). To facilitate discussion of our results, we developed a model of the *T. californica* nAChR α-γ binding site based upon the structure of the AChBP (Fig. 7). The amino acids identified by affinity labeling and mutagenesis as contributors to the ACh binding site of the nAChR are located at each subunit interface, with amino acids of segments A, B, and C contributed from one subunit and amino acids from segments D, E, and F from the other. Secondary structure elements are identified by the ribbon representation and key binding site side chains depicted in ball and stick representation. After energy minimization of the AChBP model backbone containing the primary sequences of the extracellular regions of the *T. californica* nAChR subunits, no significant movement was noted for the structures containing the amino acids of binding site segments A-E. As discussed in "Materials and Methods", the size of the insertions in the segment F region of the γ- or δ-subunit prohibits any confident prediction of the position of those insertions, and we do not depict amino acids from this region in our model of the binding site. With that caveat, the most prominent structure changes between the ACh binding site of the AChBP and the model of the *T. californica* nAChR binding site were due to single amino acid substitutions, primarily within segment E.

The binding site is a pocket lined by aromatic side chains from αTyr-93, αTrp-149, αTyr-190, αTyr-198, and γTrp-55. αTyr-93 and αTrp-149 are positioned in segments immediately after β-strands (AChBP β4 and β7, respectively). αTyr-190 and αTyr-198 are on the same side of antiparallel β-strands (AChBP β9 and β10) with the turn formed by the αCys-192/193 disulfide, which also contributes to the top of the binding pocket. The side chains of the amino acids identified from γ-subunit segments E (γLeu-109, γTyr-111, γTyr-117, and γLeu-119) and D (γTrp-55, γGlu-57) are on a com-

mon surface of three adjacent β-strands (AChBP β5′, β6, β2) which form a β sheet extending to β1 that includes γLys-34, an affinity determinant for agonists (Prince and Sine, 1996) and for α-conotoxin M1, a peptide antagonist (Sine et al., 1995; Bren and Sine, 2000). As predicted from the results of affinity labeling and mutagenesis (Chiara et al., 1999; LeNovere et al., 1999), the segment E amino acids are on antiparallel β strands with a three-amino-acid turn centered on γAsp-113. Whereas γTrp-55 contributes to the base of the pocket, the side chains of γLeu-109, γTyr-111, and γTyr-117 form part of the entrance to the pocket. γLeu-119, a position identified by Cys mutagenesis of mouse nAChR as important for α-bungarotoxin binding (Sine, 1997; Osaka et al., 2000), is the side chain from segment E that projects closest to the aromatic side chains forming the binding pocket, and the turn at γAsp-113 is most distant (~20 Å) from the aromatic pocket. While the positions of segment F agonist/antagonist affinity determinants are not included in Fig. 7, their distances from the center of the aromatic binding pocket are described in *Materials and Methods*.

The subunit primary structure of the AChBP is most closely related to the extracellular domain of nAChR α-subunits; as a homopentamer, it is more similar in structure to the α7 homopentameric neuronal nAChR than to the muscle-type nAChR. It has yet to be determined whether the AChBP undergoes conformational changes analogous to those seen with the nAChR. Because the AChBP binds ACh with reasonably high affinity (K = 4 μM) (Smit et al., 2001), it is plausible that its binding site structure differs from that of the nAChR in the resting (closed channel) state, which has low affinity for agonist, and is more similar to that of the nAChR in either the desensitized or open channel states, which bind ACh with high affinity.

Discussion

In this study, we have determined the accessibility for modification of individually substituted cysteines within segments C (α195–201) and E (γ106–113) and have further assessed their accessibility in the presence of the competitive antagonist dTC. We previously identified αY93C, αN94C, αY198C, and γE57C as accessible for modification (Sullivan and Cohen, 2000). Similar to the results obtained for segments A and D, within segment E, only two positions (γN107C, γL109C) were clearly identified by our assay as accessible for modification. Within segment C, all of the positions tested demonstrated accessibility for modification, except for αL199C. The pattern of protection by dTC identifies residues within the binding site likely to be in close proximity to bound dTC, and the selective protection of residues within segment C identifies the surface of a β-strand projecting into the dTC/agonist binding site. With the availability of a model of the *T. californica* nAChR extracellular domain, based upon the AChBP structure, it becomes possible to evaluate our results to identify consistencies and differences between the model and the structure of the nAChR binding site in the absence of agonist.

Modification of Substituted Cysteines within Segments C and E. Our studies in segment C complement previous studies in which functional embryonic mouse Cys mutant nAChRs (α183–197) were expressed on the cell surface and accessible for modification by a thiol-specific biotin, with the exception of αY190C (Spura et al., 2000). We found that ACh responses were readily quantified for each mutant *T. californica* nAChR containing Cys substitutions within α195–201, and all residues within α195–201, with the exception of αL199C, were accessible for modification. For most of these positions, introduction of either a primary amine (after MTSEA reaction) or quaternary amine (after MTSET or MBTA reaction) caused an altered response to ACh rather than an irreversible inhibition of binding. For the αY93C, γE57C, and αY198C receptors, earlier results indicated that covalent modification prevented the binding of ACh. Clearly, direct radioligand binding studies are required to determine the equilibrium constants for ACh binding to the modified Cys mutant nAChRs.

For the Cys substitutions within γ106–113 of segment E, ACh responses were modified after MTSEA or MTSET reaction with γN107C and γL109C. Reaction of the γY111C nAChR with any of the reagents had no effect on ACh responses. This was surprising, because γTyr-111 is photola-

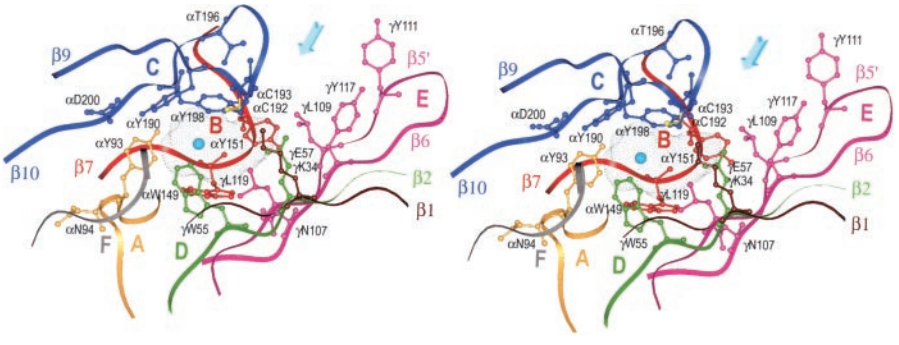

Fig. 7. Stereo representation of the *T. californica* nAChR agonist binding site at the interface between the α- and γ-subunits. A homology model of the *T. californica* nAChR was constructed from the known three-dimensional structure of the molluscan AChBP. The β-sheet regions of the model are denoted by the numbering system for the AChBP (β1, β2, etc.). A stereo representation of the ACh binding site is presented in ball and stick representation of side chains identified by affinity labeling or mutational analyses, including the Cys substitutions described in this report. The amino acids identified are in binding site segments A (αTyr-93 and αAsn-94, gold), B (αTrp-149 and αTyr-151, red), C [αTyr-190, αCys-192/193 disulfide (yellow), αThr-196, αTyr-198, and αAsp-200, blue], D (γTrp-55 and γGlu-57, green), and E (γAsn-107, γLeu-109, γTyr-111, γTyr-117, and γLeu-119, magenta). A section of the segment F ribbon is included (gray) as well as γLys-34 on β1 (brown). An ACh molecule (dotted Connolly surface) is shown within the site. After energy minimization, the ACh nitrogen, represented by the cyan sphere, is equidistant (~5 Å) from the aromatic side chains of γTrp-55, αTrp-149, αTyr-190, and αTyr-198 and 6 Å from αTyr-93. The acetyl group protrudes into the opening between segments C and E with the carbonyl oxygen oriented toward γLeu-119. The arrow denotes the likely route of ligand access.

beled by [^{3}H]dTC and is a dTC affinity determinant (Chiara et al., 1999). However, substitution of γTyr-111 by arginine had no effect on ACh equilibrium binding affinity or on the concentration dependence of channel activation, and it is quite likely that MTSET (or MBTA) may have reacted with γY111C without altering the ACh response.

dTC Protection and Binding Site Structure. Because our functional assay identified modification of substituted cysteines in segments A (αY93C, αN94C), C (α196–201, except αL199C), D (γE57C), and E (γN107C, γL109C), we wanted to determine how dTC binding altered the accessibility of cysteines for modification. If bound dTC sterically occluded access of MTSET to a binding site Cys, the rate of reaction would be reduced in proportion to dTC occupancy. Within segment C, dTC protected substituted cysteines from alkylation at α196, α198, and α200 but it did not protect α197 or α201. This dTC protection pattern is readily explained if this portion of segment C were organized as a β-strand with the side chains of α196, α198, and α200 on a common surface projecting toward the dTC/ACh binding site, as is seen in the structure of the molluscan AChBP (Brejc et al., 2001) and in the nAChR binding site model (Fig. 7, blue).

The fact that dTC protects αY198C, γE57C, and γL109C from modification but not αY93C or αN94C is consistent with the results of [^{3}H]dTC photolabeling, where there was no detectable incorporation of [^{3}H]dTC into αTyr-93 but there was photoincorporation into αTyr-198, γTrp-55, and γTyr-111. In addition, substitutions at αTyr-93 did not alter dTC affinity (Sine et al., 1994). However, within the AChBP and *T. californica* nAChR homology model binding sites, αTyr-93 forms one of the walls deep within the binding pocket along with the side chains from αTyr-190, αTyr-198, αTrp-149, and γTrp-55. Based upon that structure, we would expect dTC to protect αY93C from modification (but not αN94C, located beyond the pocket). There are potential explanations why dTC did not protect αY93C from modification. First, in the structure of the binding site based upon the AChBP, inspection of the water accessible surface (Connolly surface, not shown) indicates that there is also significant accessibility to the tyrosyl side chain from outside the pocket that may provide alternative access for modification of αY93C as well as αN94C by MTSET. Alternatively, the orientation of segment C in the nAChR binding site may be displaced from that in the model, because αCys-192/193 in the model would actually prevent dTC access to αTyr-190 or γTrp-55 within the pocket. dTC also binds to the AChBP with high affinity (Smit et al., 2001), and it was noted that for dTC to have access to the aromatic pocket, the binding site would have to open up, perhaps by a movement of the β-hairpin β9–β10 that contains segment C residues (Brejc et al., 2001).

Although our results demonstrate clearly that αD200C is accessible for modification, αAsp-200 in our model and the equivalent amino acid in the AChBP are actually in an interior position with very little surface accessibility. The rate constant for modification of αD200C by MTSET is only 1% of that of αT196C or αY198C; for modification by MBTA, however, k_{D200C} is 10-fold higher than k_{Y198C}. The rate constant for modification of αD200C by MBTA is 50-fold higher than k_{D200C} for MTSET or MTSEA. It is possible that the structure of the AChBP predicts accurately the accessibility of αAsp-200 in the nAChR and that the accessibility we see for αD200C results from a structural perturbation caused by the substitution. However, for αD200C the K_{app} for ACh is similar to wild-type, and we think it is more likely that the reactivity observed for αD200C is evidence that the accessibility of αAsp-200 is quite different than predicted from the AChBP structure and may vary in a ligand-dependent manner. Our results suggest that, in the absence of agonist, the aromatic pocket of the nAChR binding site has a more relaxed structure such that αD200C is accessible. This would happen if, for example, the antiparallel β-strands containing the segment C amino acids are further from the other elements of the binding pocket. Previous studies have provided evidence for ligand-dependent changes in the structure of the binding site. The αCys-192/193 disulfide in native *T. californica* nAChR was readily reduced by dithiothreitol in the absence of ligands or in the presence of dTC or other antagonists, but in the presence of Ach or other full agonists, the rate constant for reduction was reduced 100-fold (Damle and Karlin, 1980). Photolabeling patterns for [^{3}H]p-(*N*,*N*-dimethyl)aminobenzenediazonium in the resting and desensitized states of the nAChR provided evidence that in the two conformations the positions of αTyr-93 and αTrp-149 must differ relative to the segment C residues (Galzi et al., 1991). In addition, there is evidence that αAsp-200 is involved in an agonist dependent change in structure. Analysis of the functional consequences of the αD200N substitution in mouse nAChRs indicates that the substitution can affect the rate constant for channel opening (Akk et al., 1996) as well as the equilibrium between the resting and desensitized states (Osaka et al., 1998).

Agonist Activation. Early studies with native nAChRs established that bromoacetylcholine acted as a covalent agonist after reduction of the αCys-192/193 disulfide (Damle and Karlin, 1978; Chabala and Lester, 1986). We established previously that covalent modification of αY198C with MTSET, MTSPT, or bromoacetylcholine resulted in the addition of a covalent agonist (Sullivan and Cohen, 2000). Reaction with either MTSET or MTSPT at other segment C residues tested resulted only in inhibition of ACh responses. Thus, interactions of the tethered trimethylammonio at a distance of ~7 Å from the Cys-SH of αY198C can result in receptor activation, and this interaction is not accessible from other substituted cysteines within α195–201. This conclusion assumes that the naturally occurring disulfide bond at αCys192–193 formed in the αY198C mutant and that there was not aberrant disulfide bond formation leaving αCys192 or αCys193 as free sulfhydryls. On studies with mouse nAChR αY198C, the maximal current response was potentiated 2-fold after treatment with 1 mM dithiothreitol (McLaughlin et al., 1995), raising the possibility of aberrant disulfide bond formation that was relieved in a reducing environment. Serine substitution at αY198 causes a shift of ~300-fold in agonist binding affinity, similar to that seen with Cys substitution (Sine et al., 1994); therefore, the ~100-fold increase in αY198C K_{app} for ACh that we observed is not itself an indicator of aberrant disulfide bond formation. Under our experimental conditions, both wild-type and αY198C *T. californica* nAChRs showed a decrease (~50%) in current response, tested at half-maximal ACh concentrations, after treatment with 1 mM dithiothreitol (data not shown), thus providing no evidence for unnatural disulfide bond formation in the αY198C *T. californica* mutant.

In the future, it will be interesting to extend these studies in the context of this structural model. To further define the

requirements necessary for receptor activation, reagents with longer tethering arms, either with additional methylenes or via tethered acylcholine itself, will be tested on residues likely to project into the pocket (αP194, αT196, γL119). It will also be important to map the binding site surface protected by agonists, as well as by competitive antagonists smaller than dTC, and to determine the changes in accessibility and protection patterns when the binding site structure is altered allosterically by desensitizing noncompetitive antagonists.

References

Akabas MH and Karlin A (1995) Identification of acetylcholine receptor channel-lining residues in the M1 segment of the α-subunit. *Biochemistry* **34:**12496–12500.

Akabas MH, Kaufmann C, Archdeacon P, and Karlin A (1994) Identification of acetylcholine receptor channel-lining residues in the entire M2 segment of the alpha subunit. *Neuron* **13:**919–927.

Akk G, Sine S, and Auerbach A (1996) Binding sites contribute unequally to the gating of mouse nicotinic alpha D200N acetylcholine receptors. *J Physiol (Lond)* **496:**185–196.

Arias HR (2000) Localization of agonist and competitive antagonist binding sites on nicotinic acetylcholine receptors. *Neurochem Int* **36:**595–645.

Brejc K, van Dijk WJ, Klaassen R, Schuurmans M, van der Oost J, Smit AB, and Sixma TK (2001) Crystal structure of AChBP reveals the ligand-binding domain of nicotinic receptors. *Nature (Lond)* **411:**269–276.

Bren N and Sine SM (2000) Hydrophobic pairwise interactions stabilize alpha-conotoxin MI in the muscle acetylcholine receptor binding site. *J Biol Chem* **275:**12692–12700.

Chabala LD and Lester HA (1986) Activation of acetylcholine receptor channels by covalently bound agonists in cultured rat myoballs. *J Physiol (Lond)* **379:**83–108.

Chiara DC and Cohen JB (1997) Identification of amino acids contributing to high and low affinity d-tubocurarine sites in the *Torpedo* nicotinic acetylcholine receptor. *J Biol Chem* **272:**32940–32950.

Chiara DC, Xie Y, and Cohen JB (1999) Structure of the agonist-binding sites of the *Torpedo* nicotinic acetylcholine receptor: affinity-labeling and mutational analyses identify gamma Tyr-111/delta Arg-113 as antagonist affinity determinants. *Biochemistry* **38:**6689–6698.

Corringer P-J, Le Novere N, and Changeux J-P (2000) Nicotinic receptors at the amino acid level. *Annu Rev Pharmacol Toxicol* **40:**431–458.

Czajkowski C, Kaufmann C, and Karlin A (1993) Negatively charged amino acid residues in the nicotinic receptor delta subunit that contribute to the binding of acetylcholine. *Proc Natl Acad Sci USA* **90:**6285–6289.

Damle V and Karlin A (1978) Affinity labeling of one of two α-neurotoxin binding sites in acetylcholine receptor from *Torpedo californica*. *Biochemistry* **17:**2039–2045.

Damle VN and Karlin A (1980) Effects of agonists and antagonists on the reactivity of the binding site disulfide in acetylcholine receptor from *Torpedo californica*. *Biochemistry* **19:**3924–3932.

Galzi JL, Revah F, Bouet F, Menez A, Goeldner M, Hirth C, and Changeux J-P (1991) Allosteric transitions of the acetylcholine receptor probed at the amino acid level with a photolabile cholinergic ligand. *Proc Natl Acad Sci USA* **88:**5051–5055.

Kao P, Dwork AJ, Kaldany RJ, Silver ML, Wideman J, Stein S, and Karlin A (1984) Identification of the α-subunit half-cystine specifically labeled by an affinity reagent for the acetylcholine receptor binding site. *J Biol Chem* **259:**11662–11665.

Karlin A and Akabas MH (1998) Substituted-cysteine accessibility method. *Methods Enzymol* **293:**123–145.

LeNovere N, Corringer P-J, and Changeux J-P (1999) Improved secondary structure predictions for a nicotinic receptor subunit: incorporation of solvent accessibility and experimental data into a two-dimensional representation. *Biophys J* **76:**2329–2345.

Martin M, Czajkowski C, and Karlin A (1996) The contributions of aspartyl residues in the acetylcholine receptor gamma and delta subunits to the binding of agonists and competitive antagonists. *J Biol Chem* **271:**13497–13503.

Martin MD and Karlin A (1997) Functional effects on the acetylcholine receptor of multiple mutations of gamma Asp174 and delta Asp180. *Biochemistry* **36:**10742–10750.

McLaughlin JT, Hawrot E, and Yellen G (1995) Covalent modification of engineered cysteines in the nicotinic acetylcholine receptor agonist-binding domain inhibits receptor activation. *Biochem J* **310:**765–769.

Osaka H, Malany S, Molles BE, Sine SM, and Taylor P (2000) Pairwise electrostatic interactions between alpha-neurotoxins and gamma, delta, and epsilon subunits of the nicotinic acetylcholine receptor. *J Biol Chem* **275:**5478–5484.

Osaka H, Sugiyama N, and Taylor P (1998) Distinctions in agonist and antagonist specificity conferred by anionic residues of the nicotinic acetylcholine receptor. *J Biol Chem* **273:**12758–12765.

Prince RJ and Sine SM (1996) Molecular dissection of subunit interfaces in the acetylcholine receptor. Identification of residues that determine agonist selectivity. *J Biol Chem* **271:**25770–25777.

Prince RJ and Sine SM (1998) The ligand binding domains of the nicotinic acetylcholine receptor, in *The Nicotinic Acetylcholine Receptor: Current Views and Future Trends* (Barrantes FJ ed) pp 31–59, Springer, New York

Sine SM (1993) Molecular dissection of subunit interfaces in the acetylcholine receptor: identification of residues that determine curare selectivity. *Proc Natl Acad Sci USA* **90:**9436–9440.

Sine SM (1997) Identification of equivalent residues in the gamma, delta, and epsilon subunits of the nicotinic receptor that contribute to alpha-bungarotoxin binding. *J Biol Chem* **272:**23521–23527.

Sine SM, Kreienkamp HJ, Bren N, Maeda R, and Taylor P (1995) Molecular dissection of subunit interfaces in the acetylcholine receptor: identification of determinants of α-conotoxin M1 selectivity. *Neuron* **15:**205–211.

Sine SM, Quiram P, Papanikolaou F, Kreienkamp HJ, and Taylor P (1994) Conserved tyrosines in the alpha subunit of the nicotinic acetylcholine receptor stabilize quaternary ammonium groups of agonists and curariform antagonists. *J Biol Chem* **269:**8808–8816.

Smit AB, Syed NI, Schaap D, van Minnen J, Klumperman J, Kits KS, Lodder H, van der Schors RC, van Elk R, Sorgedrager B, et al. (2001) A glia-derived acetylcholine-binding protein that modulates synaptic transmission. *Nature (Lond)* **411:**261–268.

Spura A, Riel RU, Freedman ND, Agrawal S, Seto C, and Hawrot E (2000) Biotinylation of substituted cysteines in the nicotinic acetylcholine receptor reveals distinct binding modes for alpha-bungarotoxin and erabutoxin A. *J Biol Chem* **275:**22452–22460.

Spura A, Russin TS, Freedman ND, Grant M, McLaughlin JT, and Hawrot E (1999) Probing the agonist domain of the nicotinic acetylcholine receptor by cysteine scanning mutagenesis reveals residues in proximity to the alpha-bungarotoxin binding site. *Biochemistry* **38:**4912–4921.

Stauffer DA and Karlin A (1994) Electrostatic potential of the acetylcholine binding sites in the nicotinic receptor probed by reactions of binding-site cysteines with charged methanethiosulfonates. *Biochemistry* **33:**6840–6849.

Sullivan DA and Cohen JB (2000) Mapping the agonist binding site of the nicotinic acetylcholine receptor. Orientation requirements for activation by covalent agonist. *J Biol Chem* **275:**12651–12660.

Wang D, Chiara DC, Xie Y, and Cohen JB (2000) Probing the structure of the nicotinic acetylcholine receptor with 4- benzoylbenzoylcholine, a novel photoaffinity competitive antagonist. *J Biol Chem* **275:**28666–28674.

Zhang H and Karlin A (1997) Identification of acetylcholine receptor channel-lining residues in the M1 segment of the beta-subunit. *Biochemistry* **36:**15856–15864.

Zhang H and Karlin A (1998) Contribution of the beta subunit M2 segment to the ion-conducting pathway of the acetylcholine receptor. *Biochemistry* **37:**7952–7964.

Address correspondence to: Dr. Jonathan B. Cohen, Department of Neurobiology, Harvard Medical School, 220 Longwood Avenue, Boston, MA 02115. E-mail: jonathan_cohen@hms.harvard.edu